

Segmenting Intracellular Distribution Images Derived by Fluorescent Dyes Using a Potts Model Hamiltonian

Dandan Hu^{*1}, Pinaki Sarder^{*2}, Peter Ronhovde¹, Sharon Bloch², Samuel Achilefu² and
Zohar Nussinov¹

¹Department of Physics, Washington University, One Brookings Drive, Campus Box 1105,
St. Louis, MO 63130

²Department of Radiology, Washington University School of Medicine, 4525 Scott Avenue,
Campus Box 8225, St. Louis, MO 63110

August 24, 2012

*Dandan Hu and Pinaki Sarder contributed equally to this work

Abstract

We apply a multiresolution community detection algorithm to perform unsupervised segmentation of complex intracellular signals derived using fluorescent dyes. In our earlier work [1], when applying our method to benchmarks, our algorithm was shown to be one of the best and to be especially suited to the detection of camouflage images. In the current manuscript, we have explored this algorithm in a more complex scenario. The current image processing problem is framed as identifying clusters with respective average fluorescent lifetimes (FLTs) against a background or “solvent” in fluorescence lifetime imaging microscopy (FLIM) images derived using NIR fluorescent dyes. We have identified significant multiresolution structures using replica correlations in these images, where such correlations are manifested by information theoretic overlaps of the independent solutions (“replicas”) attained using the proposed algorithm from different starting points. Our method is more efficient than a well-known image segmentation method based on mixture of Gaussian distributions. It offers more than 1.25 times diversity based on Shannon index than the latter method, in selecting clusters with distinct average FLTs in NIR FLIM images.

1 Introduction

Image segmentation plays a crucial role in many medical imaging applications by enhancing the detection of anatomical structures of interest. Examples of medical image segmentation methods are listed in [2], which include graph partitioning methods and normalized cuts [3,4], and mixture of Gaussian distributions (MGD) method [5], to name a few.

In this work, we propose a multiresolution “community detection” (CD) approach based on graph partitioning theory [3] to segment complex intracellular signals derived using fluorescent dyes. CD [6–11] seeks to divide groups of nodes with dense connections internally and with sparser connections between the groups. Moreover, it partitions a large physically interacting system into optimally decoupled communities. To demonstrate our approach, we have used fluorescence lifetime imaging microscopy (FLIM) data captured using near-infrared (NIR) fluorescent dyes [12], where the underlying signal describing intra-cellular distribution is complex in nature. FLIM, a promising technique for imaging molecular process, uses time-resolved measurements of fluorescence from cells and thin tissue sections to generate images of the characteristic fluorescence lifetimes (FLT) within a pixel or voxel. The FLT is the average time a molecule resides in the excited state before returning to the ground state through fluorescence emission [13].

Segmentation of the FLIM data is challenging due to the high amount of spatial and temporal noise attached to such data. Such a problem is severe for images captured using organic NIR dyes because of their low photostability, resulting in low-signal-to-noise ratio (SNR) and low-resolution images. Hence, there exists a niche to efficiently segment such data to mine the spatial structures hidden in them. In this study, we deliberately used low SNR data to determine the segmentation quality of our CD method. Although we focus on the NIR FLIM data in this report, the CD method is generally applicable to diverse imaging data.

To perform the segmentation, our multiresolution CD first investigates the optimal structure at different resolutions in the input image data. It then analyzes each of these resolutions to obtain the respective number of estimated communities and the corresponding partition strengths. Partition strength is evaluated via information correlations between independent solutions (“replicas”) starting from different initial states. This analysis determines the significant structures at which the replicas are strongly correlated. The outcome of the proposed method for the case of FLIM images is a segmented image containing distinct average FLT in each of its segments. It is noteworthy to mention that our CD method is “unsupervised” in nature. Namely, it does not employ any ground-truth as a prior knowledge to train the algorithm. In particular, the algorithm does not assume any prior knowledge of specific spatial patterns corresponding to any specific community hidden in the input data.

We have compared the performance of our proposed CD method with another image segmentation method

based on the mixture of Gaussian distributions (MGD) [5] for segmenting the NIR FLIM images. Our method proves to be more than 1.25 times diverse based on Shannon index than the latter method, in finding spatial regions with distinct average FLTs in the NIR FLIM data. A detailed biological validation of the resulting segments and their biological roles is beyond the scope of this work, since such validation varies from one biological study to another. We nevertheless argue that our proposed method is general for segmenting fluorescence microscopy images, and it can be used to generate hypotheses for future biological validation.

The study is presented as follows. In Section 2, we discuss briefly on our NIR FLIM system and the structure of the data acquired from such system. Section 3 presents our proposed multiresolution CD approach for performing segmentation of images based on their spatial information. Section 4 extends our approach for images described by both spatial and temporal information. In both of these sections, we also develop image segmentation methods based on MGD. In Section 5, we present the performance of our proposed method using NIR FLIM image of an *ex vivo* liver tissue sample of mice treated with a NIR fluorescent dye. Section 5 describes a comparison of this performance with that attained using the MGD method. We conclude in Section 6.

2 Near-Infrared Fluorescence Lifetime Imaging Microscopy

Before we present our segmentation method in detail, we briefly describe an overview of our NIR FLIM system and the structure of the acquired data [12]. Our NIR FLIM system consists of a fiber-coupled laser diode (BDL-785-SMC, Becker-Hickl, Germany), a confocal laser scanning fluorescence microscope (FV1000, Olympus, Center Valley, PA), a thermoelectrically cooled, red-enhanced photomultiplier tube (PMT) (PMC-100-20, Becker-Hickl, Germany), and a time-correlated single photon counting (TCSPC) card (SPC-730, Becker-Hickl, Germany). The laser diode operates at TEM₀₀ mode [14] and provides 785 nm excitation light. Its pulsed wave duration is nominally 60-80 ps with frequency of 50 MHz. The PMT offers a minimum photon-count rate of 5 MHz. The TCSPC card has a transit-time spread of 180 ps and a dead time of 125 ns. The single photon counting operation employs equally spaced 256 time gates of duration 16.6 ns, with an initial delay of 1.4 ns for eliminating photons from the excitation pulse in the measurement.

To capture the FLIM images, the laser light was collimated, passed through the confocal system, and focused onto the sample using a 20X, 0.95-NA objective. Single photon fluorescence from the sample was collected through the same objective and directed by a dichroic mirror toward the confocal pinhole and detected by the PMT. Residual excitation light was removed using a bandstop filter with cutoff wavelengths of 765 nm and 805 nm before the PMT. Data acquisition was performed using the TCSPC card, triggered via a synchronization signal generated by the laser driver for each laser pulse. Images were acquired by

unidirectional scanning with the excitation beam using a galvanometric mirror pair as embedded in the confocal microscope system.

To generate the input data for the segmentation methods used in this study, collected time traces captured from the NIR FLIM system were first analyzed in the SPCImage software (Becker-Hickl, Germany). It replaces time traces per pixel with the cumulative time traces computed using the target pixel and its neighboring eight pixels to increase the SNR. Maximum SNR here is typically defined by the square root of the number of photons acquired in the peak channel of the 256 time gates used to perform TCSPC acquisition [15]. The resulting data of size $128 \times 128 \times 256$ describe spatio-temporal FLT information of the target field-of-view (FOV) of the imaging sample of interest. The first two dimensions of size 128×128 describes the spatial pixel locations in this FOV. The third dimension of length 256 samples for any of these pixels describes a temporal convolution between the instrument response function (IRF) and the fluorescent decay trace of that particular pixel location. To generate a spatial two-dimensional (2D) dataset for performing the segmentation, the above-mentioned three-dimensional (3D) data were analyzed further using the SPCImage software. In each pixel location of the imaging sample, the earliest time points allow fitting of the IRF, while a single-exponential curve was sufficient to fit the subsequent falloff with time along the third dimension of length 256. A χ_r^2 fitness test determined the validity of the fit, providing χ_r^2 values < 1.5 for all pixels. The resulting data of size 128×128 describe a spatial FLT information of the target FOV of the imaging sample of interest. This report presents methods for performing spatial segmentation of both 2D and 3D FLIM data described herein.

To conduct specific examples for analyzing performances of the segmentation methods explored in this work, we imaged *ex vivo* liver tissue sample of a mice treated with an NIR fluorescent dye. The NIR FLIM data was captured using the system and methodology as described above. All animal studies were performed in compliance with the Washington University School of Medicine Animal Studies Committee requirements for the humane care and use of laboratory animals in research.

3 Segmentation of Images Described by 2D Spatial Information

This section first discusses our proposed CD method for spatially segmenting images described by 2D spatial information. We also briefly review the MGD method for segmenting such images.

3.1 Community Detection Method

We employ the multiresolution CD algorithm to investigate the optimal structure at different resolutions in the input images. We use the number of estimated communities and the information based measures to

determine the significant structures at which the “replicas” are strongly correlated. (“replicas” are defined as independent solutions of the multiresolution CD algorithm attained from different starting points.) We determine different levels of detail and resolutions by setting the resolution parameters.

We minimize a Potts model Hamiltonian for solving the CD problem [11],

$$\mathcal{H} = \frac{1}{2} \sum_{k=1}^K \sum_{i \neq j} (W_{ij} - \bar{W}) \left[\Theta(\bar{W} - W_{ij}) + \gamma \Theta(W_{ij} - \bar{W}) \right] \delta(\sigma_i, \sigma_j). \quad (1)$$

Here the number of communities (segments) K can be specified from the input or left arbitrary, allowing the algorithm to decide the number of segments K using the lowest energy solutions. The weight W_{ij} denotes the absolute FLT difference between a pixel pair formed by the i^{th} and j^{th} ($\{i, j\} \in \{1, 2, \dots, N\}$) pixels in the input image with N pixels. The Heavyside functions $\Theta(\cdot)$ “turns on” or “off” the edge designation.

$$\Theta(W_{ij} - \bar{W}) = \begin{cases} 1, & \text{if } W_{ij} > \bar{W}, \\ 0, & \text{otherwise.} \end{cases} \quad (2)$$

The Kronecker delta $\delta(\cdot)$ is given by Eq. (3),

$$\delta(\sigma_i, \sigma_j) = \begin{cases} 1, & \text{if } \sigma_i = \sigma_j, \\ 0, & \text{otherwise.} \end{cases} \quad (3)$$

In this Hamiltonian, by virtue of the $\delta(\sigma_i, \sigma_j)$ term, each spin σ_i interacts only with other spins in its own segment. The spin σ_i ($\forall \sigma_i \in \{1, 2, \dots, K\}$) defines the segment identity for the i^{th} ($i \in \{1, 2, \dots, N\}$) pixel, and the algorithm optimizes it in minimizing the energy defined by Eq. (1). As such, the resulting model is *local* — a feature that enables high accuracy along with rapid convergence [10]. As before, minimizing the Hamiltonian of Eq. (1) corresponds to identifying strongly connected segments of pixels.

For the 2D NIR FLIM images, we define the weight of any edge formed by two pixels as the absolute difference between their FLTs. We then apply the multiresolution CD algorithm to segment the network formed using the image pixels as nodes. We then analyze the number of the respective estimated segments K and the replicas’ information theoretic measures (normalized mutual information I_N and variation of information V) as a function of the resolution parameter γ . Decreasing γ , the minima of Eq. (1) lead to solutions progressively lower intra-community edge densities, effectively “zooming out” toward larger

structures. We determine all natural network resolutions by identifying the values of γ for which the replicas exhibit extrema in the average information theoretic overlaps when expressed as a function of γ [9]. For more detail see [1].

3.2 Mixture of Gaussian Distribution Method

The MGD based segmentation method models the data to be a mixture of multivariate Gaussian distributions of unknown means and covariances [5]. For 2D FLIM data, FLTs of all the pixels are assumed to be a mixture of univariate Gaussian distributions of unknown means and variances, and it is segmented using the expectation maximization (EM) based optimization method for segmenting mixture of Gaussian distributions developed originally by Hastie *et al.* [5]. We discuss below the MGD method for the general case of mixture of multivariate Gaussian distributions, assuming that the number of models is known. We then present how we propose using this method specifically for the 2D data as described in Section 2.

The MGD method models the probability density function (pdf) of the k^{th} ($\forall k \in \{1, 2, \dots, K\}$) component of the data \mathbf{x} ($\mathbf{x} \in \mathbb{R}^d$) as Eq. (5), where K is the number of models defined by the number of Gaussian distributions in the mixture, d is the dimension of the data, and $\boldsymbol{\mu}_k$ of size $d \times 1$ and $\boldsymbol{\Sigma}_k$ of size $d \times d$ are the mean and covariance of the k^{th} component. Assuming the weight of the k^{th} component as a_k , the mixture pdf is given by, Eq. (4).

$$f(\mathbf{x}) = \sum_{k=1}^K a_k f_k(\mathbf{x}), \quad (4)$$

where

$$f_k(\mathbf{x}) = \frac{1}{\sqrt{(2\pi)^d |\boldsymbol{\Sigma}_k|}} \exp \left(-\frac{(\mathbf{x} - \boldsymbol{\mu}_k)^T \boldsymbol{\Sigma}_k^{-1} (\mathbf{x} - \boldsymbol{\mu}_k)}{2} \right). \quad (5)$$

To estimate the segment identity for the observed incomplete data $\{\mathbf{x}_1, \mathbf{x}_2, \dots, \mathbf{x}_N\}$, where N is the sample size, we define complete data for performing the EM based optimization as $\{(\mathbf{x}_1, y_1), (\mathbf{x}_2, y_2), \dots, (\mathbf{x}_N, y_N)\}$. Here y_i ($\forall y_i \in \{1, 2, \dots, K\}$) is the unknown segment identity of sample \mathbf{x}_i ($\forall i \in \{1, 2, \dots, N\}$). The other unknown parameters $\boldsymbol{\theta}$ includes a_k , $\boldsymbol{\mu}_k$, and $\boldsymbol{\Sigma}_k$ ($k \in \{1, 2, \dots, K\}$). The maximum likelihood function is given by Eq. (6),

$$L(\{\mathbf{x}_1, \mathbf{x}_2, \dots, \mathbf{x}_N\} | \boldsymbol{\theta}) = \sum_{i=1}^N \log \left(\sum_{k=1}^K a_k f_k(\mathbf{x}_i) \right). \quad (6)$$

A classification EM algorithm developed by Hastie *et al.* maximizes Eq. (6). To segment a 2D NIR FLIM image, we segment the collection of the FLTs $\{x_1 = \tau_1, x_2 = \tau_2, \dots, x_N = \tau_N\}$ from all the pixels of this image using the univariate version ($d = 1$) of the MGD algorithm. For simplicity, we assume K to be known, and perform the segmentation for increasing number of segments K . The final segmented image is generated using the K for which each of the resulting segments contain at least a predefined number of pixels, see Section 5.

4 Segmentation of Images Described by 3D Spatio-Temporal Information

This section extends the methods developed in Section 3 for spatially segmenting images described by 3D spatio-temporal information.

4.1 Community Detection Method

For spatially segmenting images described by 3D spatio-temporal signatures, we propose to apply multiresolution CD method in two steps. In the first step, the multiresolution CD method identifies strongly-correlated replicas in the images based on their temporal signature, and finds hidden spatial structures in them. Here if a pixel pair is always in the same community (segment) in all the replicas, they must have a strong preference to be part of the same segment or have a large edge weight. Similarly, if a pixel pair is not always in the same segment in all the replicas, they must have a preference not to be part of the same segment in all replicas or have a small edge weight. The resulting edge weights are in turn used in the second step to perform another multiresolution CD to spatially segment the target image. This strategy incorporates both the intensity and FLT information to determine spatial structures automatically in 3D FLIM data described by a spatio-temporal information.

To differentiate the proposed approach with the general image segmentation method developed in our earlier work [1], we note that the method described in [1] first generates R replicas by permuting a ‘symmetric’ initial state defined by one pixel per segment of the studied system. It then applies the CD algorithm to each replica, and records the segment membership for each pixel. In contrast, for the images described by 3D spatio-temporal signatures in this manuscript, the multiresolution CD method described in Section 3.1 considers the spatial 2D frames of this 3D data as series of replicas, and segments each of them in its first step. Namely, each replica is represented by a frame corresponding to each temporal location of the 3D FLT data. The weight of each pixel pair is calculated based on the statistics of replicas, details of which are

described below.

For performing the multiresolution CD in the second step, we define the edge weight p_{ij} between the i^{th} and j^{th} ($\{i, j\} \in \{1, 2, \dots, N\}$) pixels of the input 3D image as follows,

$$p_{ij} = \frac{1}{R} \sum_{r=1}^R \delta_{\sigma_i^r \sigma_j^r}, \quad (7)$$

where

$$\delta_{\sigma_i^r \sigma_j^r} = \begin{cases} 1, & \text{if pixel } i \text{ and } j \text{ belong to the same segment in replica } r, \\ 0, & \text{otherwise.} \end{cases} \quad (8)$$

Using Eq. (7), we redefine the analogous Hamiltonian of Eq. (1) as,

$$\mathcal{H} = \frac{1}{2} \sum_{k=1}^K \sum_{i \neq j} (\bar{p} - p_{ij}) \left[\Theta(p_{ij} - \bar{p}) + \gamma \Theta(\bar{p} - p_{ij}) \right] \delta(\sigma_i, \sigma_j), \quad (9)$$

which we minimize for performing the multiresolution CD.

4.2 Mixture of Gaussian Distribution Method

For performing the MGD based segmentation using the 3D spatio-temporal data, we normalize each temporal data corresponding to pixel i ($\forall i \in \{1, 2, \dots, N\}$) in 2D spatial location to form $\mathbf{x}_i = [x_{i1}, x_{i2}, \dots, x_{id}]^T$, where $d = 256$ in our case, see Section 2. The normalization here ensures $\max \{x_{il} \mid l \in \{1, 2, \dots, d\}\} = 1$. The resulting \mathbf{x}_i ($i \in \{1, 2, \dots, N\}$) are used to perform the multivariate MGD as discussed in Section 3.2.

5 Results

This section describes representative examples of the proposed multiresolution CD method using an *ex vivo* liver tissue sample treated using an NIR fluorescent dye. We also compare the performance of our proposed method with the MGD method.

5.1 Multiresolution Community Detection for Varying γ

For the FLIM image of the liver tissue shown in Fig. 1A, we define the edge weight between two pixels as the absolute FLT difference between them. We applied the multiresolution CD to solve the resulting network formed by the image pixels as nodes. Fig. 1B shows the plots of the information theoretic overlaps between

the replicas of the multiresolution CD, such as their normalized mutual information I_N and variation of information V , together with the number of estimated segments \hat{K} as a function of the resolution parameter γ . Decreasing γ , the minima of Eq. (1) leads to solutions with progressively lower intra-segment edge densities, effectively “zooming out” toward larger structures. We determine all natural network resolutions by identifying the values of γ for which the replicas exhibit extrema in the average of their information theoretic overlaps when expressed as a function of γ . The extrema and plateau of the average information theoretic overlaps as a function of γ over all replica pairs indicate the natural network resolutions [9].

Figs. 1C-1G show the image segmentation results by our multiresolution CD algorithm at different resolutions. As the resolution decreases from Fig. 1C to 1G, the images show less detailed structures. In Fig. 1C, three segments are clearly visible (light blue, green, and orange), in addition to the background segment (brown). In Fig. 1G, only one segment (light orange) appears against the background (light blue). Figs. 1D-1F show the results produced using the multiresolution CD algorithm with the ranges of γ that are in between the ones used for generating Figs. 1C and 1G. The segmented images show two distinct segments located in the background. Thus by using different resolutions γ , the multiresolution CD method is able to detect the structures at different scales.

5.2 Performance for Images Described by 2D Spatial Information

We then compare in Fig. 2 the multiresolution CD method with the MGD method for the 2D spatial data of the FLIM image shown in Fig. 1A. In Figs. 2A and 2C, we present the image segmentation results by the MGD and multiresolution CD, respectively. Note that we evaluated the former method here for increasing number of segments K , and for $K > 3$, the method started producing segments with pixels fewer than 100. In contrast, the multiresolution CD method selects the number of segments automatically as discussed in Sections 3.1 and 4.1. In the current example, we used $\gamma \in (0.6, 0.7)$ for performing segmentation using this method. To measure the performances of the two methods, we plot in Figs. 2B and 2D the respective normalized average decay traces as the function of photon arrival time in the PMT. The proposed multiresolution CD method is able to identify segments with more distinct and diverse decay traces than the other method as seen in these two plots. This method allows the user to adjust the resolution γ , and thus to obtain the segments with more distinct and diverse decay traces.

To quantify the diversity offered by the respective segmentation methods, we compute the Shannon index for each of them. Shannon index has been widely used in the literature to quantify species diversity in a habitat or community [16]. We compute this index for our study using the set described by the Euclidean distances between every pairs of average decay traces of the estimated segments for MGD or multiresolution

CD method. To perform this computation, we first bin the computed distances using intervals defined by $(0.2(m-1), 0.2m]$, where $m \in \{1, 2, \dots, M\}$ and

$$M = \left\lceil \frac{\max(\tilde{d}_{\text{MGD}}, \tilde{d}_{\text{MCD}})}{0.2} \right\rceil, \quad (10)$$

where $\lceil \cdot \rceil$ denotes a ceiling function and \tilde{d}_{MGD} and \tilde{d}_{MCD} are the maximum computed Euclidean distances between the average decay traces of the estimated segments for MGD and multiresolution CD methods, respectively. We then compute the frequency of occurrence of the distances in each bin, and denote this frequency by q_m for the m^{th} bin. We finally compute the Shannon index for MGD or multiresolution CD method as,

$$H = - \sum_{m=1}^M q_m \log q_m. \quad (11)$$

We obtained $H_{\text{MGD}} = 0.64$ and $H_{\text{MCD}} = 1.26$ for the MGD based and multiresolution CD based segment estimates of the 2D spatial data of the FLIM image shown in Fig. 1A. This result suggests that the multiresolution CD method offers almost more than two times diversity than the MGD method in segmenting FLIM images described by 2D spatial information.

5.3 Performance for Images Described by 3D Spatio-Temporal Information

We finally compare in Fig. 3 the multiresolution CD with the MGD method for the 3D spatio-temporal version of the FLIM image shown in Fig. 1A. In Figs. 3A and 3C, we present the image segmentation results by the MGD and multiresolution CD, respectively. The optimal number of segments was selected respectively by the MGD method and the CD method using the similar procedures as stated in Sections 3 and 4. To conduct the segmentation using the multiresolution CD on the 3D spatio-temporal data, we used single resolutions in both steps; particularly, we used $\gamma_1 = 1$ and $\bar{V}_1 = 2.5$ in its first step and $\gamma_2 = 10$ and $\bar{V}_2 = 2.5$ in its second step. Both of the methods are able to produce more connected structures for the 3D spatio-temporal data than was obtained for the 2D spatial data. The resulting normalized average decay traces of the estimated segments are shown in Fig. 3B and 3D for the respective methods. For a clearer depiction, Fig. 3D here shows the decay traces only for segments with number of pixels more than 300. To quantify the diversity offered by the respective segmentation methods, we computed $H_{\text{MGD}} = 1.1$ and $H_{\text{MCD}} = 1.53$ for the MGD based and multiresolution CD based segment estimates of the 3D spatio-temporal version of the FLIM image shown in Fig. 1A. This result suggests that the multiresolution CD method offers almost more than 1.25 times diversity than the MGD method in segmenting FLIM images described by 3D

spatio-temporal information.

6 Conclusion

We have developed a multiresolution community detection algorithm to segment two-dimensional and three-dimensional fluorescence lifetime imaging microscopy (FLIM) data. The proposed method is able to identify structures in different scales in the input FLIM images based on an information theoretic measures. It offers atleast 1.25 times more diversity based on Shannon index than a state-of-the art method based on mixture of Gaussian distributions, in producing distinct and diverse decay traces in the segmented images.

Acknowledgement

This work is supported by the National Science Foundation (NSF) under grant number NSF DMR-1106293 and by the National Institute of Health (NIH) under grant number NIH R01 EB008111, NIH R01 EB007276, NIH R33 CA123537, NIH U54 CA136398, and NIH HHSN268207000046C.

A Definitions: Trials and Replicas

We review the notions of “trials” and “replicas,” used in our community detection (CD) algorithms. Both of these notions pertain to the use of multiple identical copies of the same system which differ from one another by a permutation of the initial site indices. Thus, whenever the time evolution depends on sequentially ordered searches for energy lowering moves (as it does in our greedy algorithm), these copies may generally reach different local solutions. By the use of an ensemble of such identical copies, we attain accurate results as well as determine information theoretic correlations between the candidate solutions, and infer from them a detailed picture of the system.

In the definitions of “trials” and “replicas” given below, any given algorithm may be used to minimize the selected cost function. In our particular case, we minimize the Hamiltonian of Eq. 1.

- Trials: We use “trials” alone in our bare community detection algorithm. We run the algorithm on the same problem T independent times. This may generally lead to different contending states that minimize Eq. 1. Out of these T trials, we pick the lowest energy state and use that state as the solution.
- Replicas: We use both “trials” and “replicas” in our multiresolution CD algorithm. Each sequence of the above described T trials is termed as a replica. When using “replicas” in the current context, we run the aforementioned T trials (and pick the solution that attains lowest energy in the Hamiltonian of Eq.

1) R independent times. By examining information theoretic correlations between the R replicas, we infer which features of the contending solutions are well agreed on (and thus are likely to be correct), and on which features there is a large variance between the disparate contending solutions that may generally mark important physical boundaries. We compute the information theoretic correlations within the ensemble of R replicas. Specifically, the information theoretic extrema as a function of the resolution parameter, generally correspond to more pertinent solutions that are locally stable to a continuous change of scale. It is in this way we detect the important physical scales in the system.

B Information Theoretic Measures

We use information theoretic measures to calculate correlations between community detection (CD) solutions. The CD method partitions N pixels for a replica r ($\forall r \in \{1, 2, \dots, R\}$) into K_r segments, where segment k ($k \in \{1, 2, \dots, K_r\}$) consists of N_k pixels. The ratio N_k/N is the probability that a randomly selected pixel is found in the segment k ($k \in \{1, 2, \dots, K_r\}$). The Shannon entropy [11] is

$$H_r = - \sum_{k=1}^{K_r} \frac{N_k}{N} \log_2 \frac{N_k}{N}. \quad (12)$$

The mutual information $I(r, s)$ between the replicas r and s ($\{r, s\} \in \{1, 2, \dots, R\}$) is

$$I(r, s) = \sum_{k_1=1}^{K_r} \sum_{k_2=1}^{K_s} \frac{N_{k_1 k_2}}{N} \log_2 \frac{n_{k_1 k_2} N}{n_{k_1} n_{k_2}}, \quad (13)$$

where $N_{k_1 k_2}$ is the number of common pixels in the segment k_1 ($k_1 \in \{1, 2, \dots, K_r\}$) of replica r ($r \in \{1, 2, \dots, R\}$) and the segment k_2 ($k_2 \in \{1, 2, \dots, K_s\}$) of replica s ($s \in \{1, 2, \dots, R\}$).

The variation of information $V(r, s)$ between the two segments r and s is

$$V(r, s) = H_r + H_s - 2I(r, s), \quad (14)$$

which has a range of $0 \leq V(r, s) \leq \log_2 N$.

The normalized mutual information $I_N(r, s)$ is

$$I_N(r, s) = \frac{2I(r, s)}{H_r + H_s}, \quad (15)$$

with the obvious range of $0 \leq I_N(r, s) \leq 1$.

Higher $I_N(\cdot)$ and lower $V(\cdot)$ values indicate better agreement between the compared segments.

C Community Detection Algorithm

Our community detection (CD) algorithm for minimizing Eq. (1) follows four steps [10].

1. We partition the pixels based on a symmetric or fixed K initialization where K is the number of segments.
 - Symmetric initialization alludes to an initialization, where each pixel forms its own segment; i.e., initially, there are $K^{(0)} = N$ segments.
 - Fixed K initialization corresponds to a random initial distribution of all pixels into K segments.

For image segmentation, a symmetric initialization is used for the unsupervised case. In this case, the algorithm does not know what the number of segments are, so the symmetric initialization provides the advantage of no bias towards a particular segment. The algorithm decides the number of segments K , by means of the lowest energy solution.

Fixed K initialization may be used in a supervised image segmentation. The community membership of an individual pixel is then changed to lower the solution energy using CD algorithm. Here the user has to decide how much information is needed by observing the original image, and enter the number of segments K as an input, where different levels of information correspond to different numbers of segments K . For instance, if only one target needs to be identified, $K = 2$ is enough, which describe the target and background.

In our work, we use the unsupervised image segmentation, and let the algorithm decide the community number K .

2. Next, we select each pixel, and place it in the segment that best lowers the energy of Eq. (1) based on the current state of the system.
3. We repeat this process for all pixels, and continue iterating until no energy lowering moves are found after one full cycle through all pixels.
4. We repeat these processes for T trials, and select the lowest energy result as the best solution. Different trials differ solely by the permuted pixel order of the initial state. In the multi-resolution application discussed below, we further use different replicas, i.e., different independent solutions attained using our proposed algorithm, and solve the system based on a finite temperature algorithm [11].

D Multiresolution Algorithm

We illustrate below how the multiresolution algorithm [9] works.

To begin the multiresolution algorithm, we need to specify the number of replicas R at each resolution, the number of trials per replica T , and the starting and ending resolutions, γ_0 and γ_f , respectively. We typically use the number of replicas as $8 \leq R \leq 12$, and the number of trials as $2 \leq T \leq 20$. We select the lowest energy solution among the T trials for each replica. The initial state of the replicas are generated by permuting the pixel labels in the symmetric initialized state of one pixel per community. These permutations P simply reorder the pixel indices $(1, 2, 3, \dots, i, \dots, N) \rightarrow (P1, P2, \dots, PN)$ (with Pi the state of i under a permutation), and thus lead to a different initial state.

1. The algorithm starts from the initialization of the system, described in item (1) of Section C.
2. We then minimize Eq. (1) independently for all replicas at a resolution $\gamma = \gamma_i \in \{\gamma_0, \gamma_1, \dots, \gamma_{f-1}, \gamma_f\}$ as described in Section C. Initially, $i = 0$ (i.e., $\gamma = \gamma_0$).
3. The algorithm then calculates the average inter-replica information theoretic measures, such as I_N and V , at that value of γ .
4. The algorithm then proceeds to the next resolution $\gamma_{i+1} \in \{\gamma_0, \gamma_1, \dots, \gamma_{f-1}, \gamma_f\}$ (with $\gamma_{i+1} > \gamma_i$).
5. We then return to Step 2.
6. After examining the case of $\gamma = \gamma_f$, the algorithm outputs the inter-replica information theory overlaps for the entire range of the resolutions studied.
7. We examine those values of γ corresponding to the extrema in the average inter-replica information theoretic overlaps. Physically, the resulting image segmentation for these values is locally insensitive to the change of resolution (i.e., small changes in γ) and generally highlights prominent features of the image.

With A and B denoting graph segments in two different replicas, and $Q(A, B)$ their overlap, the average inter-replica overlap for a general quantity $Q(\cdot)$ [9] is explicitly

$$\langle Q \rangle = \frac{1}{R(R-1)} \sum_{A \neq B} Q(A, B). \quad (16)$$

Similarly, for a single replica quantity, the average is, trivially, $\langle Q \rangle = \sum_A H(A)/R$ [9].

E Classification Expectation Maximization Algorithm

To maximize Eq. (6), we use a classification expectation maximization algorithm [5], steps of which we briefly review below. For more discussion, readers might consult the classical book on machine learning written by Hastie *et al.* [5].

1. We initialize the parameters a_k , $\boldsymbol{\mu}_k$, and $\boldsymbol{\Sigma}_k$ ($k \in \{1, 2, \dots, K\}$). To perform this initialization, we first initialize the segment identity y_i ($\forall y_i \in \{1, 2, \dots, K\}, i \in \{1, 2, \dots, N\}$) by randomly assigning its value to be 1, 2, ..., or K . We perform this random assignment here by uniformly drawing a number from $\{1, 2, \dots, K\}$, and assign this number to $y_i^{(0)}$ ($i \in \{1, 2, \dots, N\}$). Based on this assignment, we compute $a_k^{(0)}$ ($k \in \{1, 2, \dots, K\}$) as,

$$a_k^{(0)} = \frac{\sum_{i=1}^N 1(y_i^{(0)} = k)}{N}, \quad (17)$$

where $1(y_i^{(0)} = k)$ is an indicator function as given by,

$$1(y_i^{(0)} = k) = \begin{cases} 1, & \text{if } y_i^{(0)} = k, \\ 0, & \text{otherwise.} \end{cases} \quad (18)$$

Similarly, we compute $\boldsymbol{\mu}_k^{(0)}$ and $\boldsymbol{\Sigma}_k^{(0)}$ ($k \in \{1, 2, \dots, K\}$) as,

$$\boldsymbol{\mu}_k^{(0)} = \frac{\sum_{i=1}^N 1(y_i^{(0)} = k) \mathbf{x}_i}{\sum_{i=1}^N 1(y_i^{(0)} = k)}, \quad (19)$$

and

$$\boldsymbol{\Sigma}_k^{(0)} = \frac{\sum_{i=1}^N 1(y_i^{(0)} = k) (\mathbf{x}_i - \boldsymbol{\mu}_k^{(0)}) (\mathbf{x}_i - \boldsymbol{\mu}_k^{(0)})^T}{\sum_{i=1}^N 1(y_i^{(0)} = k)}. \quad (20)$$

2. Expectation step: This step computes the posterior probabilities for all $\{i = 1, 2, \dots, N\}$ and $\{k = 1, 2, \dots, K\}$ for the $(l+1)^{\text{th}}$ iteration, using updated estimates of the parameters a_k , $\boldsymbol{\mu}_k$, and $\boldsymbol{\Sigma}_k$ from the l^{th} iteration. This step determines how likely \mathbf{x}_i is to be the part of the k^{th} segment. The posterior probability is given by,

$$p_{i,k} = \frac{a_k^{(l)} f_k(\mathbf{x}_i | \boldsymbol{\mu}_k^{(l)}, \boldsymbol{\Sigma}_k^{(l)})}{\sum_{k=1}^K a_k^{(l)} f_k(\mathbf{x}_i | \boldsymbol{\mu}_k^{(l)}, \boldsymbol{\Sigma}_k^{(l)})}. \quad (21)$$

3. Classification step: This step determines for the $(l+1)^{\text{th}}$ step which among $k = 1, 2, \dots, K$ is most likely to be the segment identity of \mathbf{x}_i ($i \in \{1, 2, \dots, N\}$). Namely, we compute,

$$J_i^{(l+1)} = \underset{k}{\operatorname{argmax}} p_{i,k}, \quad (22)$$

$$\hat{p}_{i,k'} = \begin{cases} 1, & \text{if } k' = \underset{k}{\operatorname{argmax}} p_{i,k}, \\ 0, & \text{otherwise.} \end{cases} \quad (23)$$

4. Maximization step: Using the information obtained from Eqs. (16) and (17), we update the estimates of the parameters a_k , $\boldsymbol{\mu}_k$, and $\boldsymbol{\Sigma}_k$ as,

$$a_k^{(l+1)} = \frac{\sum_{i=1}^N \hat{p}_{i,k}}{N}, \quad (24)$$

$$\boldsymbol{\mu}_k^{(l+1)} = \frac{\sum_{i=1}^N \hat{p}_{i,k} \mathbf{x}_i}{\sum_{i=1}^N \hat{p}_{i,k}}, \quad (25)$$

$$\boldsymbol{\Sigma}_k^{(l+1)} = \frac{\sum_{i=1}^N \hat{p}_{i,k} (\mathbf{x}_i - \boldsymbol{\mu}_k^{(l+1)}) (\mathbf{x}_i - \boldsymbol{\mu}_k^{(l+1)})}{\sum_{i=1}^N \hat{p}_{i,k}}. \quad (26)$$

5. We repeat Steps 2-4, until convergence. The convergence is determined by

$$\frac{|L(\{\cdot\}|\boldsymbol{\theta}^{(l)}, y^{(l)}) - L(\{\cdot\}|\boldsymbol{\theta}^{(l-1)}, y^{(l-1)})|}{|L(\{\cdot\}|\boldsymbol{\theta}^{(l-1)}, y^{(l-1)})|} < \epsilon, \quad (27)$$

where ϵ is an infinitesimally small number, which was 0.001 in our case. The EM algorithm described herein monotonically increases the cost function defined by Eq. (6) [5], and the unknown parameters are guaranteed to converge, at least locally.

References

- [1] D. Hu, P. Ronhovde, & Z. Nussinov, “Replica inference approach to unsupervised multiscale image segmentation,” *Physical Review E*, vol. 85, pp. 016101, 2012.
- [2] D. L. Pham, C. Xu, & J. L. Prince, “A survey of current methods in medical image segmentation,” *Annual Review of Biomedical Engineering*, vol. 2, pp. 315, 1998.
- [3] S. Fortunato, “Community detection in graphs,” *Physics Reports*, vol. 486, pp. 75–174, 2010.
- [4] J. Shi & J. Malik, “Normalized cuts and image segmentation,” *IEEE Transactions on Pattern Analysis and Machine Intelligence*, vol. 22, pp. 888–905, 2000.
- [5] T. Hastie, R. Tibshirani, & J. H. Friedman, *The Elements of Statistical Learning: Data Mining, Inference and Prediction*, Ed. 2, Springer-Verlag, 2008.
- [6] M. Girvan & M. E. J. Newman, “Community structure in social and biological networks,” *Proceedings of the National Academy of Sciences of the USA*, vol. 99, pp. 7821–7826, 2002.
- [7] S. Fortunato, “Community detection in graphs,” *Physics Reports*, vol. 486, pp. 75–174, 2010.
- [8] M. E. J. Newman, “Detecting community structure in networks,” *European Physical Journal B*, vol. 38, pp. 321–330, 2004.
- [9] P. Ronhovde & Z. Nussinov, “Multiresolution community detection for megascale networks by information-based replica correlations,” *Phys. Rev. E*, vol. 80, pp. 016109, 2009.
- [10] P. Ronhovde & Z. Nussinov, “Local resolution-limit-free Potts model for community detection,” *Physical Review E*, vol. 81, pp. 046114, 2010.
- [11] D. Hu, P. Ronhovde, & Z. Nussinov, “Phase transition in random Potts systems and the community detection problem: Spin-glass type and dynamic perspectives,” *Philosophical Magazine*, vol. 92, pp. 406–445, 2012.
- [12] R. Nothdurft, P. Sarder, S. Bloch, J. Culver, & S. Achilefu, “Fluorescence lifetime imaging microscopy using near-infrared contrast agents,” *Journal of Microscopy*, vol. 247, pp. 202–207, 2012.
- [13] M. Y. Berezin & S. Achilefu, “Fluorescence lifetime measurements and biological imaging,” *Chemical Reviews*, vol. 110, pp. 2641–2684, 2010.
- [14] D. K. Cheng, *Field and Wave Electromagnetics*, Addison-Wesley, Boston, 1989.

- [15] M. Kollner & J. Wolfrum, “How Many Photons Are Necessary for Fluorescence-Lifetime Measurements,” *Chemical Physics Letters*, vol. 200, pp. 199–204, 1992.
- [16] C. E. Shannon, “A mathematical theory of communication,” *The Bell System Technical Journal*, vol. 27, pp. 379–423 & 623–656, 1948.

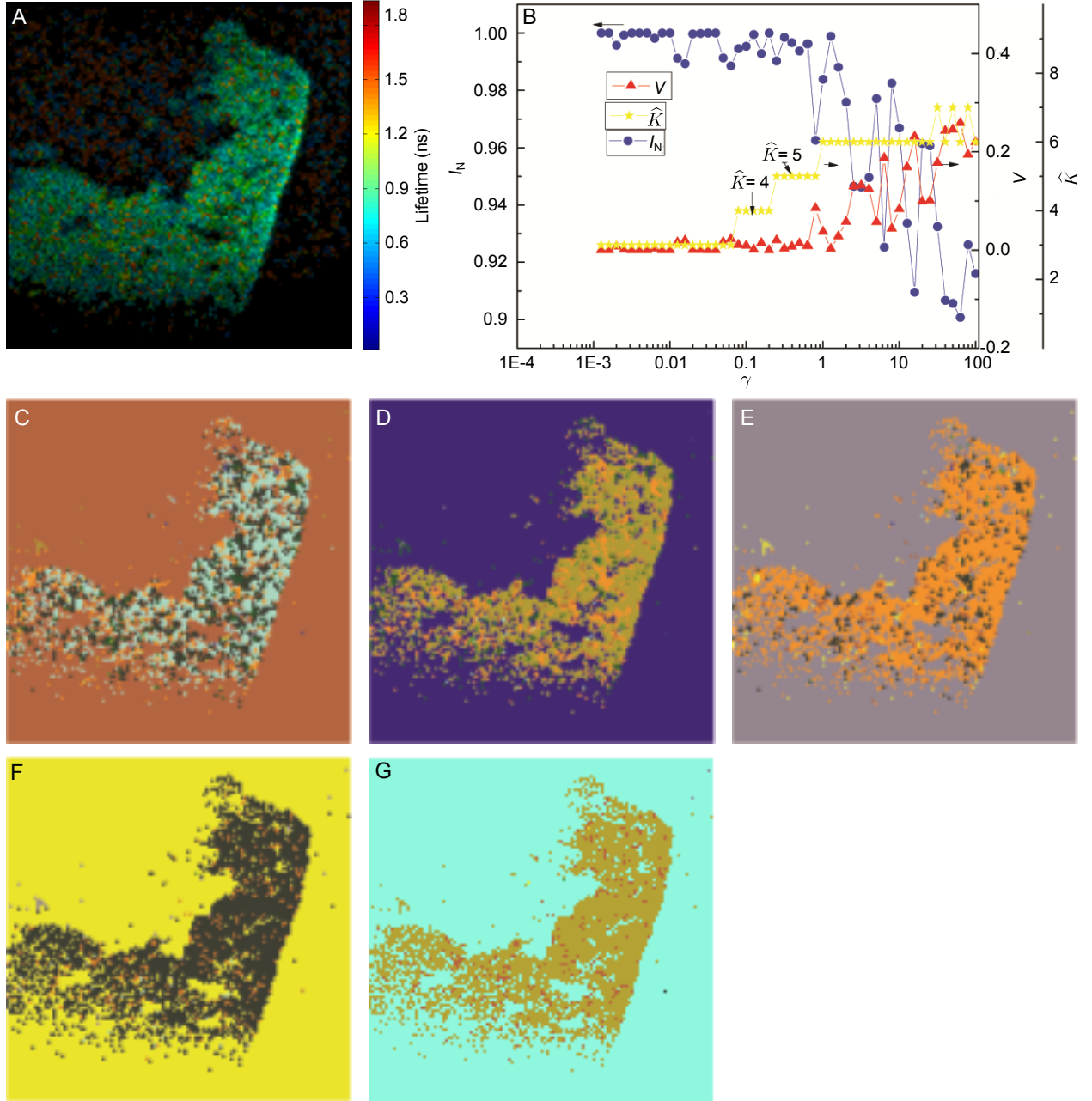


Figure 1: Segmentation results for an *ex vivo* liver tissue image with two-dimensional (2D) spatial information: Panel A shows the result generated by the multiresolution community detection (CD) method for segmenting images described by the 2D fluorescence lifetime imaging microscopy data of an *ex vivo* liver tissue sample. Panel B shows the normalized mutual information I_N and the variation of information V of the replicas of the multiresolution CD method and its number of estimated segments \hat{K} as the function of resolution parameter γ . We selected the values of γ at the peaks of the curve described using V , and obtained the segmented images as shown in Panels C-G by our proposed multiresolution CD method. Images with the higher values of γ have more precise structures, see Panels C and D. Images with the lower values of γ have rough structures, see Panels E, F, and G.

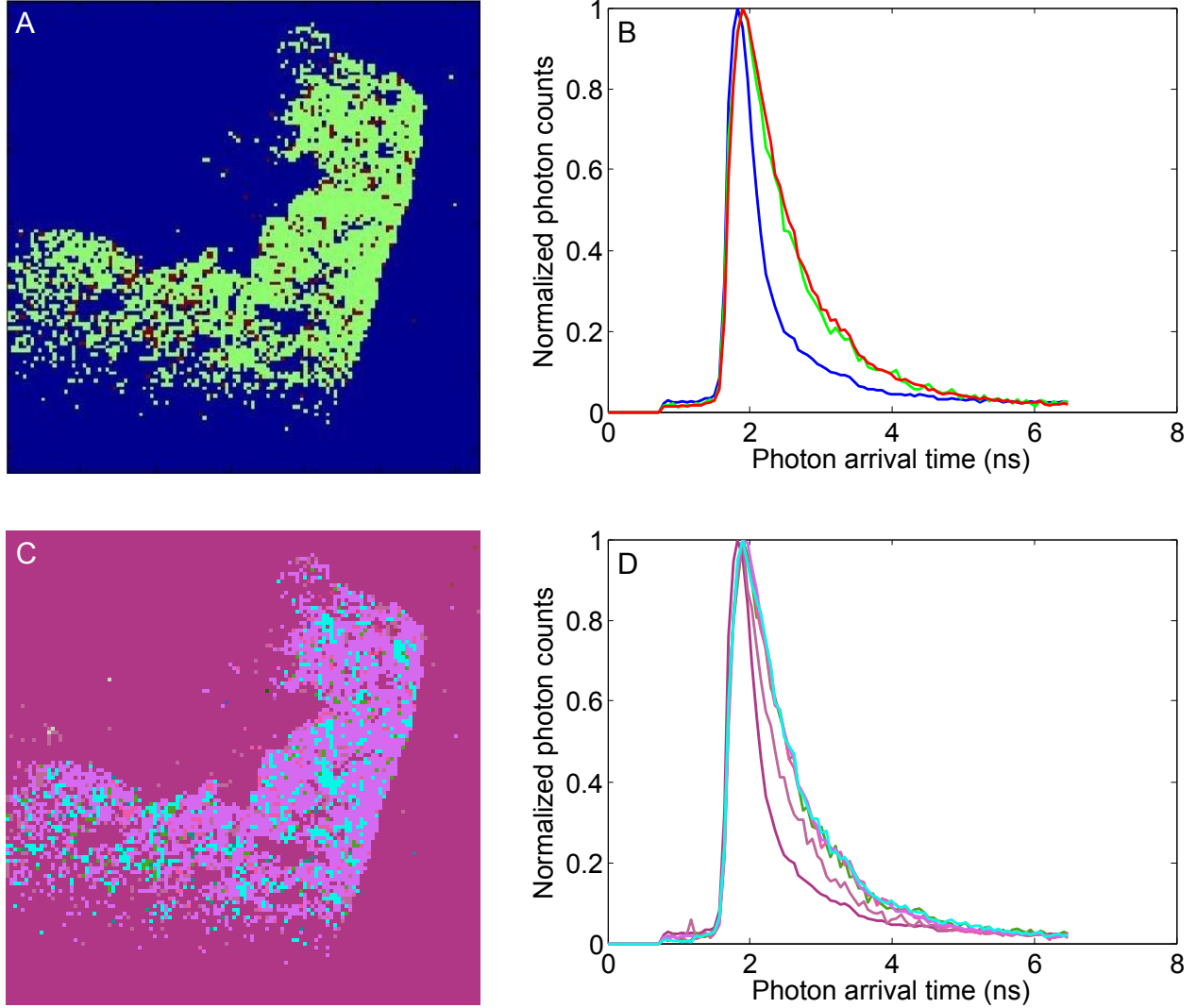


Figure 2: Comparison between the multiresolution community detection (CD) method and the mixture of Gaussian distributions (MGD) method for images described by two-dimensional spatial information: Panel A is the segmentation result by the MGD method. Panel B shows the normalized average decay traces corresponding to the estimated segments shown in Panel A. Panel C is the segmentation result by the multiresolution CD method using $\gamma = 0.7$. Panel D shows the normalized average decay traces corresponding to the estimated segments shown in Panel C. Multiresolution CD is able to identify more distinct and diverse decay traces than the MGD method.

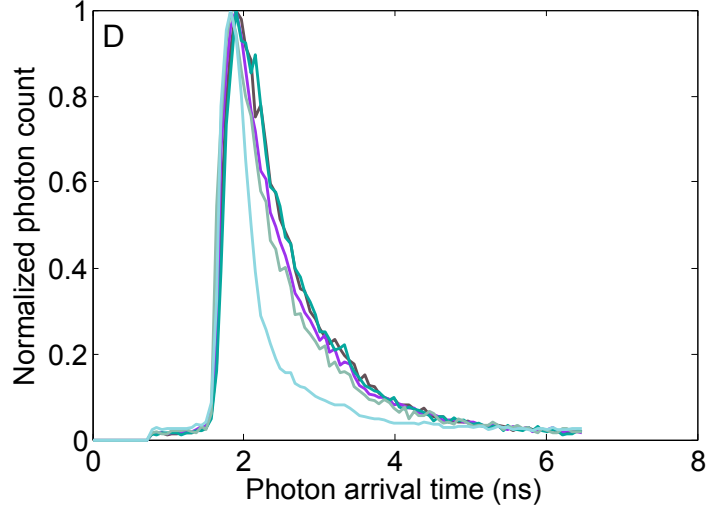
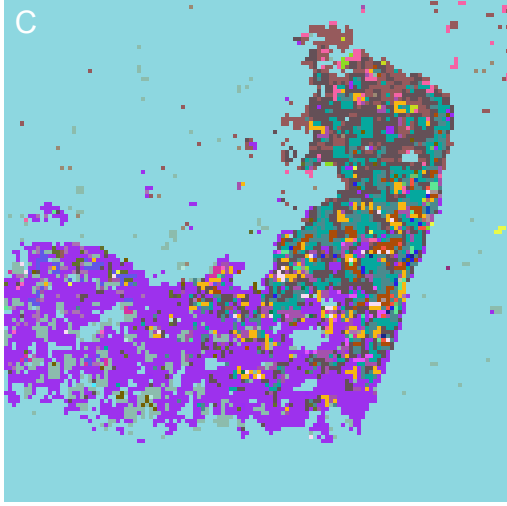
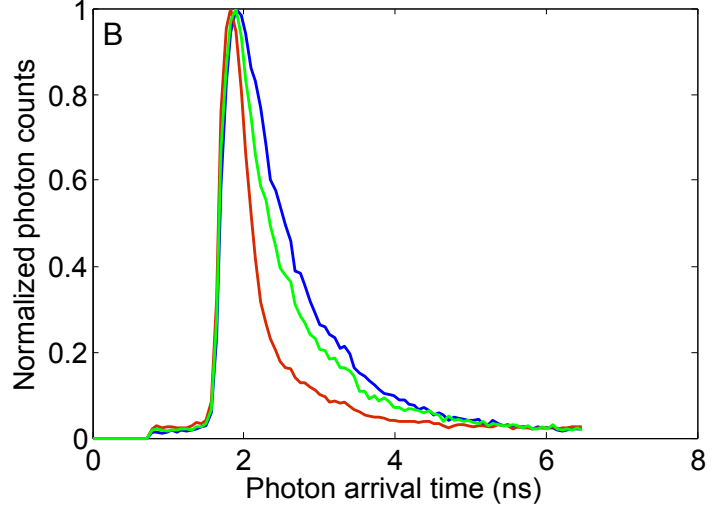
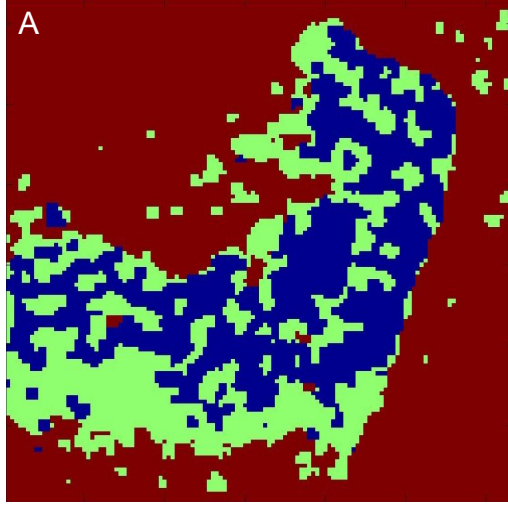


Figure 3: Comparison between the multiresolution community detection (CD) method inspired by the replica correlation and the mixture of Gaussian distributions (MGD) method for images described by three dimensional (3D) spatio-temporal information. Panel A is the result obtained by the MGD method. Panel B shows the normalized average decay traces corresponding to the estimated segments shown in Panel A. Panel C is the segmentation result by the multiresolution CD method developed for images described by 3D spatio-temporal information, using $\gamma_1 = 1$ and $\bar{V}_1 = 2.5$ in its first step and $\gamma_2 = 10$ and $\bar{V}_2 = 2.5$ in its second step. Panel D shows the normalized average decay traces corresponding to the estimated segments shown in Panel C. Both of the methods are able to produce more connected structures for the 3D spatio-temporal data than that was obtained for the 2D spatial data. Our results indicate that both of the methods here appear to be performing similarly in terms of generating segments with distinct and diverse decay traces.